Available online at www.sciencedirect.com
SCIENCE DIRECT®
ELSEVIER
International Journal of Solids and Structures xxx (2005) xxx–xxx
INTERNATIONAL JOURNAL OF SOLIDS and STRUCTURES
www.elsevier.com/locate/ijsolstr

# Structural performance of near-optimal sandwich panels with corrugated cores

L. Valdevit [a], Z. Wei [b], C. Mercer [b], F.W. Zok [b,*], A.G. Evans [b]

[a] *Division of Engineering and Applied Sciences, Harvard University, Cambridge, MA 02138, United States*
[b] *Materials Department, University of California, Santa Barbara, CA 93106-5050, United States*

Received 7 April 2005; received in revised form 15 June 2005

**Abstract**

An experimental and computational study of the bending response of steel sandwich panels with corrugated cores in both transverse and longitudinal loading orientations has been performed. Panel designs were chosen on the basis of failure mechanism maps, constructed using analytic models for failure initiation. The assessment affirms that the analytic models provide accurate predictions when failure initiation is controlled by yielding. However, discrepancies arise when failure initiation is governed by other mechanisms. One difficulty is related to the sensitivity of the buckling loads to the rotational constraints of the nodes, as well as to fabrication imperfections. The second relates to the compressive stresses beneath the loading platen. To address these deficiencies, existing models for core failure have been expanded. The new results have been validated by experimental measurements and finite element simulations. Limit loads have also been examined and found to be sensitive to the failure mechanism. When face yielding predominates, appreciable hardening follows the initial non-linearity, rendering robustness. Conversely, for designs controlled by buckling (either elastic or plastic) failure initiation is immediately followed by softening. The implication is that, when robustness is a key requirement, designs within the face failure domain are preferred.


*Keywords:* Lightweight structures; Sandwich panels; Corrugated core; Imperfection sensitivity

## 1. Introduction

All-metallic sandwich panels combine weight-efficiency (Ashby et al., 2000; Evans et al., 2001; Wadley et al., 2003) with blast containment (Fleck and Deshpande, 2004; Qiu et al., 2003, 2004; Radford et al.,

* Corresponding author. Tel.: +1 805 893 8699; fax: +1 805 893 8486.
*E-mail address:* zok@engineering.ucsb.edu (F.W. Zok).

0020-7683/$ - see front matter © 2005 Elsevier Ltd. All rights reserved.
doi:10.1016/j.ijsolstr.2005.06.073

2005; Vaughn et al., 2005; Xue and Hutchinson, 2003, 2004; Rathbun et al., in press) and, in some cases, efficient active cooling (Valdevit et al., 2004; Lu et al., 2005). Progress has been enabled by the development of a straightforward and inexpensive manufacturing technology (Sypeck and Wadley, 2001; Wadley et al., 2003). Cores of interest include honeycombs (Zok et al., in press; Cote et al., 2004), pyramidal and tetrahedral trusses (Chiras et al., 2002; Rathbun et al., 2004; Wicks and Hutchinson, 2004; Zok et al., 2004), textile meshes (Sypeck and Wadley, 2001; Zok et al., 2003) as well as corrugated and diamond ducts (Valdevit et al., 2004). Full-scale application requires that the structural performance be characterized using a combination of analytical and numerical results, validated by experiments. Such characterizations have been developed for truss and honeycomb core panels (Rathbun et al., 2004; Zok et al., 2004, in press). This article presents analogous results for panels with corrugated prismatic cores. It draws upon analytic results for minimum weight designs presented elsewhere (Valdevit et al., 2004). The assessment is presented for the two principal orientations (Fig. 1a): *transverse* (bending plane normal to the corrugation axis) and *longitudinal* (bending parallel to the axis). The geometries used for testing were chosen to be near-optimal in each. All tests have been performed on 304 stainless steel panels, fabricated by brazing. Previous assessments have indicated that the properties of this steel are affected by fabrication and that comparisons between measurements and calculations should be made using the braze-modified properties (Zok et al., 2004).

The outline of the paper is as follows. In Section 2, a synopsis of the analytical model for corrugated core panels is presented and geometries of interest are selected. Section 3 presents the experimental protocol and

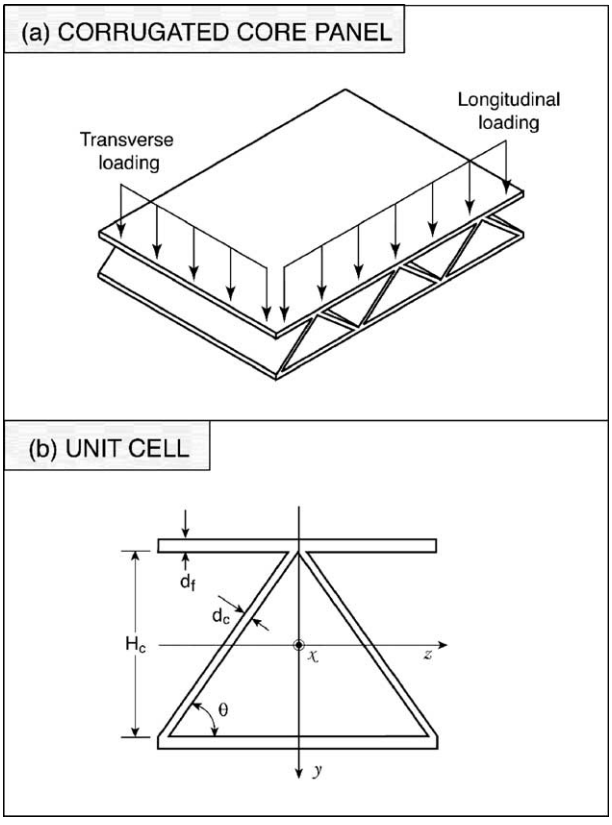


Fig. 1. Schematics of a corrugated core panel and the associated unit cell.

flexural measurements performed on panels with near-optimal configurations. The results are compared with the predictions of the analytic model and discrepancies highlighted. To address these disparities, finite element simulations are presented in Section 4.

## 2. Panel design and analysis

### 2.1. Preliminaries

The panels under consideration are depicted in Fig. 1. The geometric variables are the core thickness, $H_c$, the face sheet thickness, $d_f$, the core member thickness, $d_c$, and the corrugation angle, $\theta$. The non-dimensional loading intensity for bending is $V^2/EM$, with $E$ the elastic modulus of the material, $M$ the maximum moment and $V$ the maximum shear force. The ratio $l = M/V$ identifies the relevant length scale (Wicks and Hutchinson, 2001). Efficient structures are obtained by minimizing the weight per unit width of the panel $W$ under the constraint that the applied load remains below that needed to activate any of the failure mechanisms. From geometry, the non-dimensional weight is

$$\psi = \frac{W}{\rho l^2} = 2\frac{d_f}{l} + \frac{1}{\cos\theta}\frac{d_c}{l} \tag{1}$$

with $\rho$ the density of the material. A summary of the critical loads for failure initiation follows; their derivations have been presented elsewhere (Valdevit et al., 2004).

### 2.2. Generalized bending

Four failure mechanisms are considered: face yielding (FY), face buckling (FB) core yielding (CY) and core buckling (CB). Failure initiation loads for each are ascertained from a stress analysis, coupled with yielding and buckling criteria. Effects of indentation stresses on core failure are addressed in the subsequent section.

For the *transverse orientation*, the four critical loads are:

$$\left(\frac{V^2}{EM}\right)_{FY} = \frac{\varepsilon_Y d_f}{l}\left(\frac{H_c}{l} + \frac{d_f}{l}\right) \tag{2a}$$

$$\left(\frac{V^2}{EM}\right)_{CY} = \frac{\varepsilon_Y d_c \sin\theta}{l} \tag{2b}$$

$$\left(\frac{V^2}{EM}\right)_{FB} = \frac{k_f \pi^2 \tan^2\theta}{48}\left(\frac{H_c}{l} + \frac{d_f}{l}\right)^{-1}\left(\frac{d_f}{l}\right)^3 \tag{2c}$$

$$\left(\frac{V^2}{EM}\right)_{CB} = \frac{k_c \pi^2 \sin^3\theta}{12}\left(\frac{H_c}{l} + \frac{d_f}{l}\right)^{-2}\left(\frac{d_c}{l}\right)^3 \tag{2d}$$

where $\varepsilon_Y$ is the material yield strain. The buckling coefficients $k_f$ and $k_c$ depend on the rotational constraint offered by the adjoining members at the nodes (Bazant and Cedolin, 1991). Retaining only the contribution of the elements in tension gives conservative estimates. These are (Valdevit et al., 2004):

$$k_f = \left(\frac{2.4\cos\theta(d_c/d_f)^3 + 1}{1.2\cos\theta(d_c/d_f)^3 + 1}\right)^2 \tag{3a}$$

$$k_c = 1.375\left(\frac{2.2 + 1.2(d_f/d_c)^3/\cos\theta}{1.6 + 0.6(d_f/d_c)^3/\cos\theta}\right) \tag{3b}$$

This choice has been made because optimal designs frequently lie at the confluence of core and face buckling. In such cases, adjoining members in compression are simultaneously on the verge of buckling and offer little contribution to the rotational stiffness of the nodes. However, for designs in which the critical loads for core buckling are considerably greater than those for the face, or vice versa, the constraints offered by all members should be included. By repeating the procedures leading to the derivation of Eqs. (3) (Valdevit et al., 2004) but including the constraint offered by the members in compression, the coefficients become:

$$k_f = \left(\frac{2.2 + 4.8\cos\theta(d_c/d_f)^3}{1.6 + 2.4\cos\theta(d_c/d_f)^3}\right)^2 \tag{4a}$$

$$k_c = \left(\frac{2.2 + (1.2/\cos\theta)(d_f/d_c)^3}{1.6 + (0.6/\cos\theta)(d_f/d_c)^3}\right)^2 \tag{4b}$$

The formulae in Eqs. (3) and (4) provide bounds. That is, if the critical loads for the two buckling modes are similar, Eq. (3) should be used; otherwise, Eq. (4) provides more realistic estimates.

For *longitudinal loading*, the critical loads are (Valdevit et al., 2004):

$$\left(\frac{V^2}{EM}\right)_{FY} = \frac{\varepsilon_Y\left[\frac{d_f}{l} + \frac{1}{6\cos\theta}\frac{d_c}{l}\right]\left(\frac{H_c}{l} + \frac{d_f}{l}\right)}{\sqrt{1 + \frac{3}{\tan^2\theta}\left(\frac{H_c}{l} + \frac{d_f}{l}\right)^2}} \tag{5a}$$

$$\left(\frac{V^2}{EM}\right)_{CY} = \min_{y\in\left[0,\frac{H_c}{2}\right]}\left\{\frac{\varepsilon_Y\left(\frac{H_c}{l} + \frac{d_f}{l}\right)\left[\frac{d_f}{l} + \frac{1}{6\cos\theta}\frac{d_c}{l}\right]}{\sqrt{4\left(\frac{y}{H_c + d_f}\right)^2 + 3\left[\frac{1}{\tan\theta}\left(\frac{H_c}{l} + \frac{d_f}{l}\right)\frac{d_f}{l}\frac{l}{d_c} + \frac{1}{\sin\theta}\left(\frac{H_c}{l} + \frac{d_f}{l}\right)\left(\frac{1}{4} - \left(\frac{y}{H_c + d_f}\right)^2\right)\right]^2}}\right\} \tag{5b}$$

$$\left(\frac{V^2}{EM}\right)_{FB} = \frac{K_c\pi^2\tan^2\theta}{24(1-\nu^2)}\left(\frac{d_f}{l}\right)^2\left(\frac{H_c}{l} + \frac{d_f}{l}\right)^{-1}\left[\frac{1}{2}\frac{d_f}{l} + \frac{1}{12\cos\theta}\frac{d_c}{l}\right] \tag{5c}$$

$$\left(\frac{V^2}{EM}\right)_{CB} = \frac{\frac{\pi^2\sin^2\theta}{12(1-\nu^2)}\left(\frac{d_c}{l}\right)^2\left[\frac{d_f}{l} + \frac{1}{6\cos\theta}\frac{d_c}{l}\right]}{\left(\frac{H_c}{l} + \frac{d_f}{l}\right)\sqrt{\frac{1}{K_b^2} + \frac{1}{K_s^2}\left(\frac{H_c}{l} + \frac{d_f}{l}\right)^2\left[\frac{1}{\tan\theta}\frac{d_f}{l}\frac{l}{d_c} + \frac{1}{4\sin\theta}\right]^2}} \tag{5d}$$

where $\nu$ is Poisson's ratio and $y$ is the distance from the neutral axis (Fig. 1(b)) and min denotes the minimum value over the pertinent domain. Here the buckling coefficients are $K_c = 4$, $K_s = 5.35$ and $K_b = 23.9$.

These results allow the construction of preliminary failure maps (Fig. 2), which enable the design of near-optimal panels: one each for the longitudinal and transverse orientations. The two designs (used in the subsequent experiments) are denoted by the solid circles in Fig. 2. They differ only in their core thickness: $H_c/l = 0.055$ and 0.115. The former is selected to be nearly optimal in the transverse orientation and the latter nearly optimal in the longitudinal orientation. Slight deviations from optimality arise due to thickness restrictions on commercially available steel sheets.

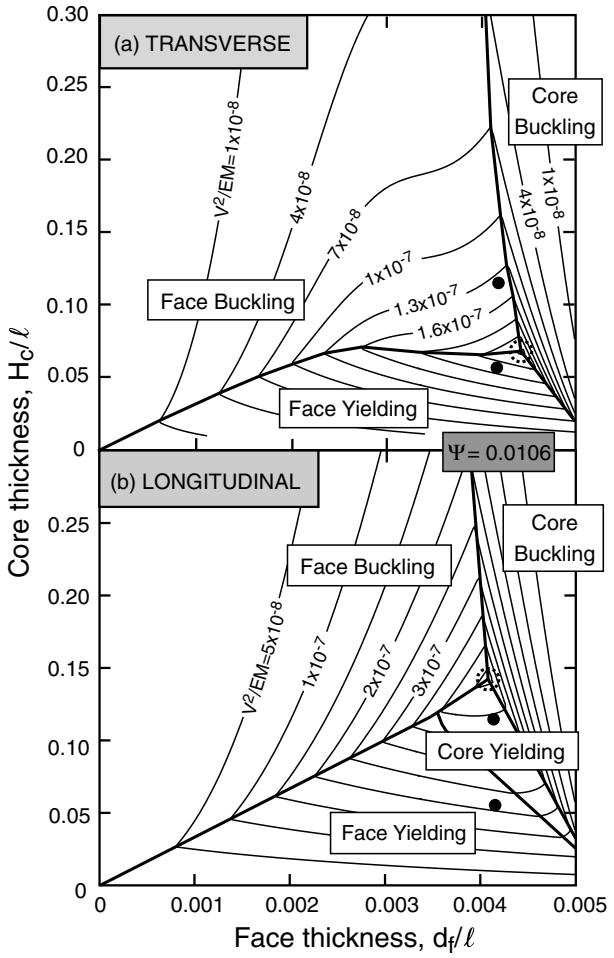


Fig. 2. Failure mechanism maps for corrugated core panels, neglecting indentation stresses (panel weight, $\psi = 0.0106$; corrugation angle, $\theta = 45°$; yield strain, $\varepsilon_Y = 0.0008$).

### 2.3. Indentation

The preceding results have the deficiency that the compressive stresses induced by the loading platen have not been included. Such stresses can play a significant role in core failure, as demonstrated in the subsequent experimental study. To address this limitation, the following approach is adopted. (Details are presented in Appendix A.)

(a) An analytic model is used to estimate the core indentation stress beneath a loading platen of width $2a$ in a three-point bending specimen. Comparison with a three-dimensional finite element calculation of one of the designs is used to assess the accuracy.
(b) The indentation stress is combined with that due to bending and the Mises criterion used to predict yield. The result follows a form similar to that in Eq. (5b), but with additional terms due to indentation. The lower of the two loads (with and without indentation) is chosen.

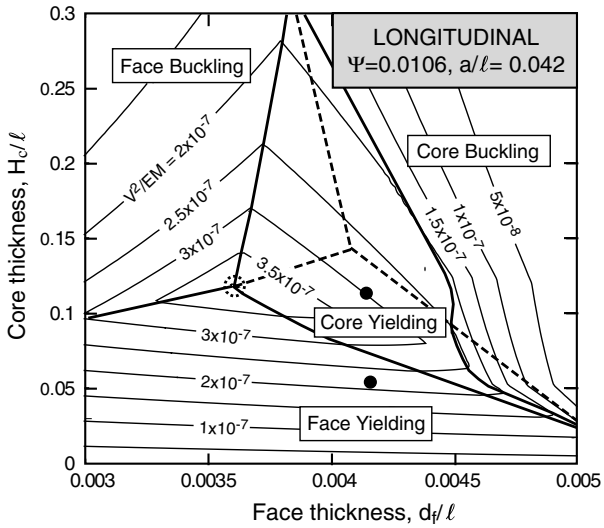


Fig. 3. Modified failure mechanism map for longitudinal loading, accounting for indentation stresses. Boundaries of original map (neglecting indentation—Fig. 2(b)), are shown by the dashed lines. Dashed lines denotes optimal design.

(c) The indentation stress is used to predict buckling of the core members. The new buckling load is compared with that due to bending alone; the lower one is chosen.
(d) The modified results for core failure are combined with those for face failure (Eqs. (5a) and (5c)) to recompute the mechanism boundaries and the load capacities.

A modified failure mechanism map based on the preceding protocol is presented in Fig. 3. Results are plotted for $a/l = 0.042$: chosen to be representative of the experiments described below. Note that the indentation stress expands the domain over which core failure mechanisms are active. It also causes a shift in the optimal design to lower values of both core thickness and face thickness. Comparisons with the subsequent experimental measurements are used to further assess these predictions.

## 3. Experimental assessment

### 3.1. Panel design and testing

Near-optimal panels designed in accordance with Fig. 2 have been fabricated from 304 stainless steel, using methods described elsewhere (Sypeck and Wadley, 2001; Wadley et al., 2003; Zok et al., 2004). Briefly, the cores were produced by sequentially bending flat plates along the lines of the nodes through an angle of 45°. The cores were subsequently bonded to the face sheets by brazing, using a mixture of a polymer-based cement (Nicrobraz Cement 520) and a Ni–22Cr–6Si braze powder (Nicrobraz 31), both supplied by Wal Colmonoy (Madison Heights, MI). All geometric parameters are given in Table 1. The beams were tested in three-point flexure with a loading span $S = 300$ mm. The load $P$ was applied through a 12.7 mm wide platen. To assess reproducibility, two samples of each configuration were tested under nominally identical conditions.

Table 1
Geometric parameters of the two panel designs

| $d_f$ (mm) | $d_c$ (mm) | $H_c$ (mm) | $l$ (mm) | $d_f/l$ | $d_c/l$ | $H_c/l$ | $\theta$ (°) |
|---|---|---|---|---|---|---|---|
| 0.635 | 0.25 | 17.5 | 152.4 | 0.00417 | 0.0016 | 0.115 | 45 |
| 0.635 | 0.25 | 8.4 | 152.4 | 0.00417 | 0.0016 | 0.055 | 45 |

### 3.2. Measurements and observations

The load–deflection curves measured for the two different orientations are presented in non-dimensional coordinates in Fig. 4. Images at significant stages in the deformation are presented in Fig. 5. Note that, in most cases, the limit loads measured on the two equivalent panels are consistent (Fig. 4) and deformation modes are the same (Fig. 5). The exception is the thicker panel tested transversely. For this design, while one panel failed by face buckling, the other failed by core buckling at lower load. These differing responses are addressed in Section 4.

To provide context, it is instructive to compare the results with those for a monolithic beam of the same areal density. At failure initiation, the latter is given by (Zok et al., 2003):

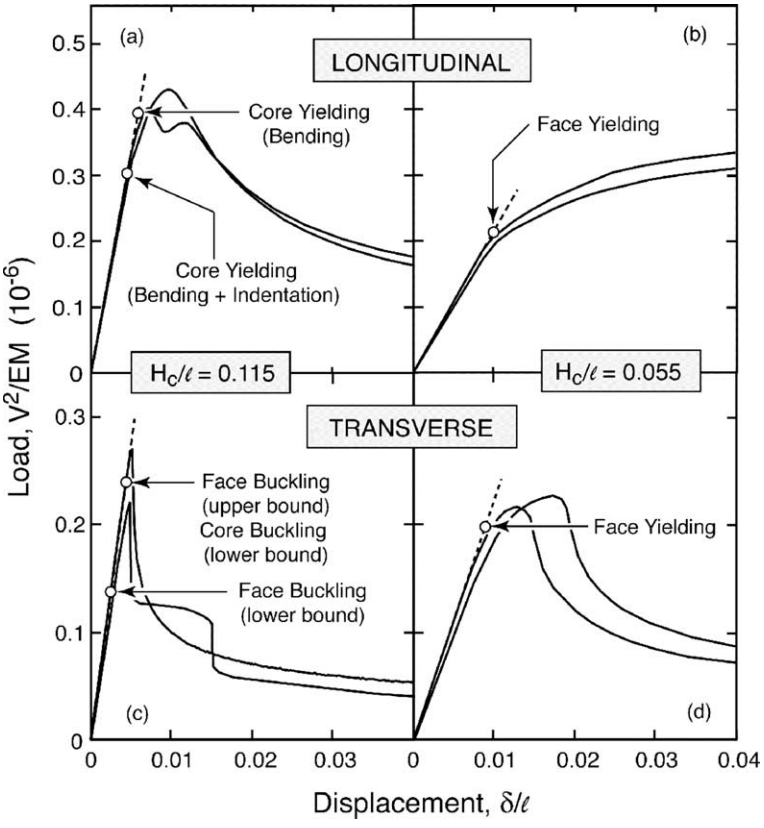


Fig. 4. Experimental bending results for all test specimens, along with analytic failure predictions (open circles). In (c), the upper bound estimate for face buckling coincides (fortuitously) with the lower bound for core buckling.

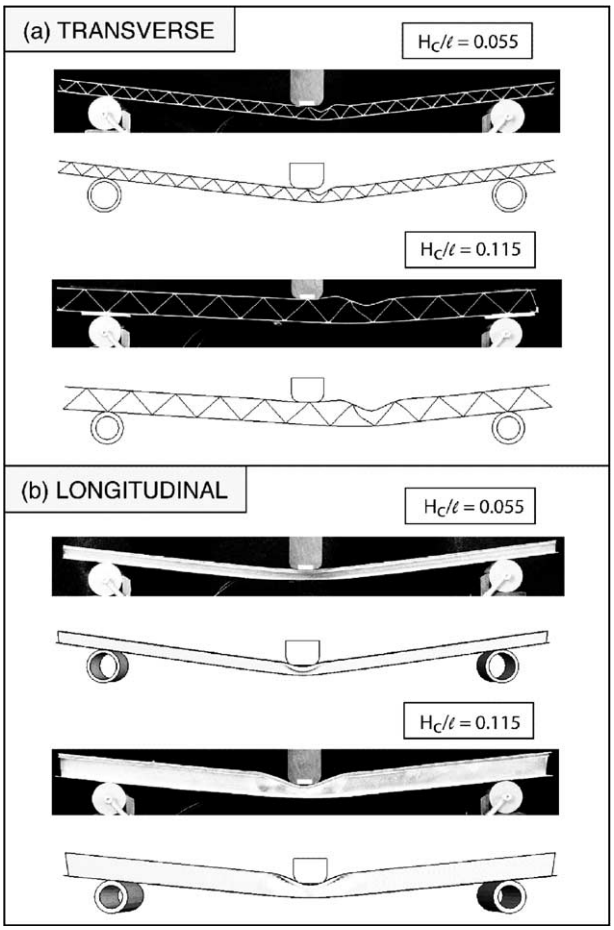


Fig. 5. Comparisons of deformation modes obtained experimentally and through numerical simulations.

$$\left(\frac{V^2}{EM}\right)_{\mathrm{MY}} = \frac{\varepsilon_{\mathrm{Y}}\Psi^2}{6} \tag{6}$$

For the pertinent properties ($\varepsilon_{\mathrm{Y}} = 0.0008$ and $\Psi = 0.0106$), the load at failure initiation, $(V^2/EM)_{\mathrm{MY}} \approx 1.5 \times 10^{-8}$, is more than an order of magnitude below those for the sandwich panels.

Note that the thinner panel loaded longitudinally exhibits the most desirable response (Fig. 4(b)). In this panel, failure initiation occurs by face yielding, at $V^2/EM \approx 2 \times 10^{-7}$, followed by appreciable hardening (plastic buckling in the core is deferred to large plastic displacements). All other panels exhibit comparable or slightly higher critical loads ($V^2/EM \approx (2\text{–}3) \times 10^{-7}$), but undergo dramatic softening just beyond the criticality, because buckling is the active failure mechanism (Fig. 2) (either elastic buckling for the thicker panel tested in the transverse direction, or plastic buckling just after yield for the two remaining panels).

### 3.3. Assessment

The analytic predictions for the failure initiation loads, obtained from Section 2, are superimposed on the measurements in Fig. 4. The interpretation for the *thinner panels* is straightforward. The predicted loads (Fig. 4(b) and (d)), governed by face yielding, are consistent with the measurements, provided the yield

strength (160 MPa) of brazed 304 stainless steel is used (Zok et al., 2004). The interpretation for the *thicker panels* (Fig. 4(a) and (c)) is more nuanced. It requires that comparisons be conducted with several analytic solutions: two buckling options for transverse loading (Eqs. (3) and (4)) and two core response models for longitudinal loading (with and without indentation). For the *longitudinal orientation*, the indentation result based on core yield coincides most closely with the measured loads. The results associated solely with bending (neglecting indentation) is non-conservative, by about 30%. In the *transverse orientation*, the lower bound for face buckling is grossly conservative, by almost a factor of 2. The upper bound lies between the two peak loads obtained in the experiments.

Differences in failure mode for the two thicker panels in the transverse orientation are addressed through select finite element calculations, presented in the next section. The calculations provide a more complete appreciation for the expected load capacities as well as the ensuing plastic response.

## 4. Finite element analysis

### 4.1. Model

A numerical study has been performed using the finite element code ABAQUS©. The meshes are depicted in Fig. 6. In all cases, three-dimensional reduced integration shell elements (S4R) were used. The

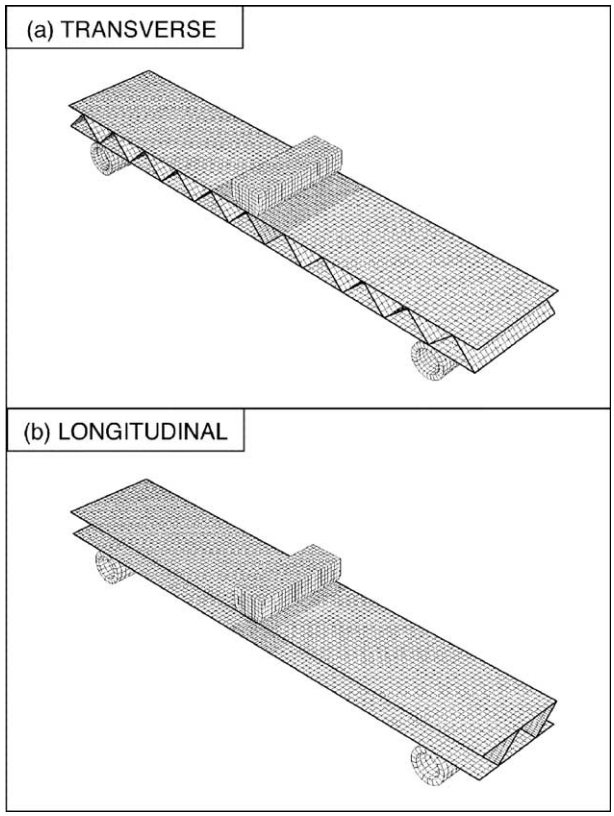


Fig. 6. Representative finite element meshes for both transverse and longitudinal loading orientations. Shell elements are used to represent the panels, whereas solid elements are used for the central loading platen and the rollers.

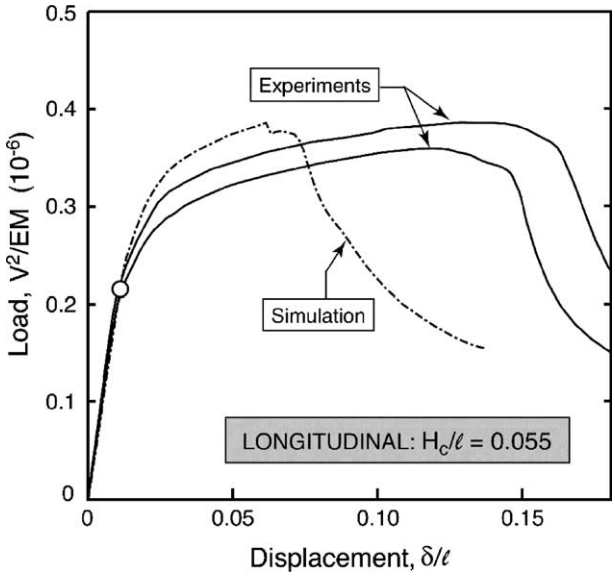


Fig. 7. Load–displacement curves for the thinner panel tested in the longitudinal direction. The open circle indicates the analytic prediction for face yielding. Note the differences in the displacement scale used here and in Figs. 8–10. This design and orientation yields the best post-yield response by a large margin.

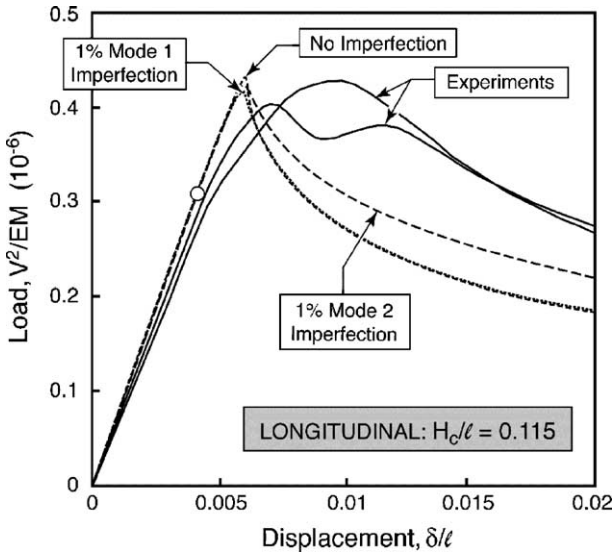


Fig. 8. Load–displacement curves for the thicker panel tested in the longitudinal direction. Note the weak imperfection sensitivity relative to that shown in Figs. 9 and 10. The eigenmodes are presented in Fig. 12. The open circle indicates the onset of core yielding beneath the platen.

mesh was denser in the region around the central platen. The rollers were modeled with reduced integration eight-node solid elements (C3D8R). Contacts between the panel and the rollers as well as between the panel and the platen were modeled as hard surfaces (no penetration), with a friction coefficient of 0.1. The rollers

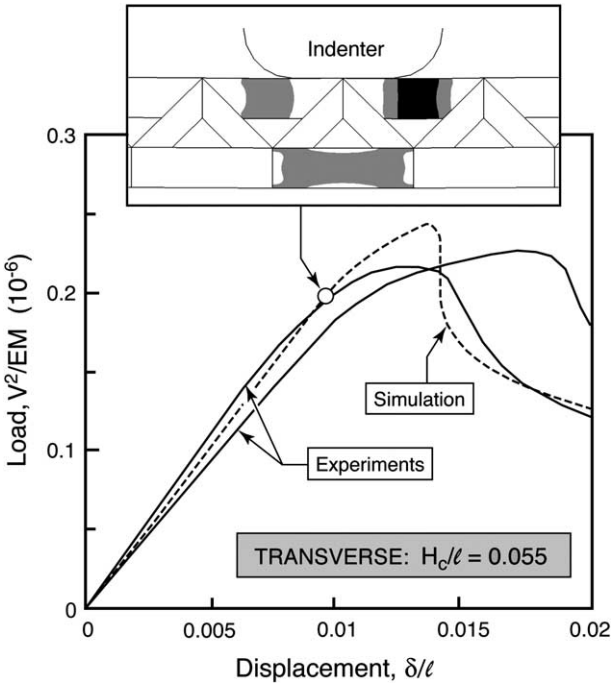


Fig. 9. Load–displacement curves for the thinner panel tested in the transverse direction. Inset shows the plastic region (shaded) at the onset of non-linearity, confirming failure initiation by face yielding.

were clamped at their centers. One node of the panel was restrained horizontally. The stress/strain curve measured for brazed 304 stainless steel was used to characterize the plastic response (Young's modulus, $E = 200$ GPa, Poisson ratio, $v = 0.3$, yield strength, $\sigma_Y = 160$ MPa, yield strain, $\varepsilon_Y = \sigma_Y/E = 0.0008$). The load–displacement behavior was obtained by imposing a vertical displacement on the platen.

### 4.2. Load/deflection curves

The simulated load/deflection curves are presented in Figs. 7–10. Generally, the load capacities (limit loads) correspond closely with the measurements. But, the calculated plastic displacements are generally lower than the measurements, sometimes significantly (Fig. 7). This disparity remains unresolved.

The failure modes for the thicker panels under *transverse loading* are elaborated by conducting an eigenvalue analysis to extract the lowest energy buckling modes. The first four buckling modes are presented in Fig. 11, together with the associated critical loads. Note that face buckling is the lowest mode, consistent with the analytic prediction. This mode occurs in one test (Fig. 10(a)): but, core buckling (mode 3) occurs in the other, even though it requires a higher load (Fig. 11). Introducing small mode 3 imperfections (characterized by the ratio of lateral displacement to member length) and recalculating the load/deflection responses gives the results summarized in Fig. 10(b). Note that an imperfection with 1% amplitude is sufficient to modify the order of the eigenvalues and trigger failure by core buckling. A 2% imperfection predicts loads consistent with the experimental result. Moreover, by introducing mode 1 imperfections and recalculating the response, now failure occurs by face buckling. *The implication is that the responses found in practice can differ among beams in a manner dictated by fabrication imperfections.*

The corresponding analysis for the *longitudinal orientation* (Fig. 12) reveals the first four modes. Choosing the two lowest and introducing imperfections results in the load/deflection responses in Fig. 8. In all

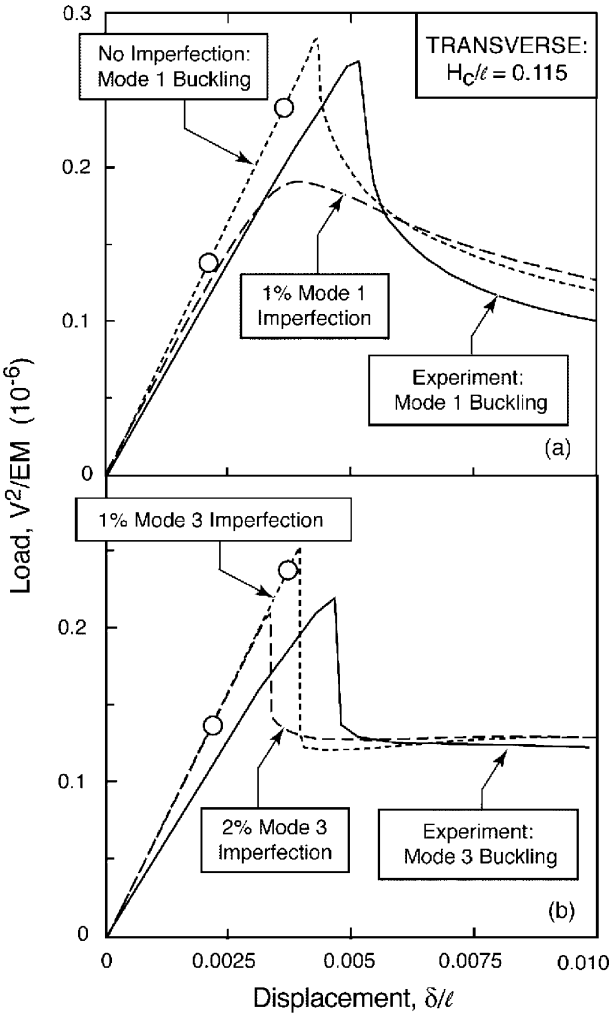


Fig. 10. Load–displacement curves from both experiments and FE calculations for the thicker panel tested in the transverse direction. Eigenmodes are reported in Fig. 11. The open circles represent analytic bounds for face buckling. In (a), the test specimen failed by face buckling (mode 1); the buckling load predicted by FE (without imperfection) agrees well the measured peak value. In (b), failure occurred by core buckling (mode 3). Here the buckling load is consistent with a 2% mode 3 imperfection.

cases, buckling is preceded by core yielding beneath the indenter, at a load $V^2/EM = 0.32 \times 10^{-6}$. This value is essentially the same as that from the analytic model that incorporates indentation, shown in Fig. 4(a). In contrast with the transverse orientation, the load capacity is imperfection insensitive. This may be due in part to the plasticity that precedes buckling.

## 5. Conclusions and implications

An experimental and computational study of the mechanical response of sandwich plates with corrugated cores has been performed. The goals have included the assessment of analytic models of beam failure

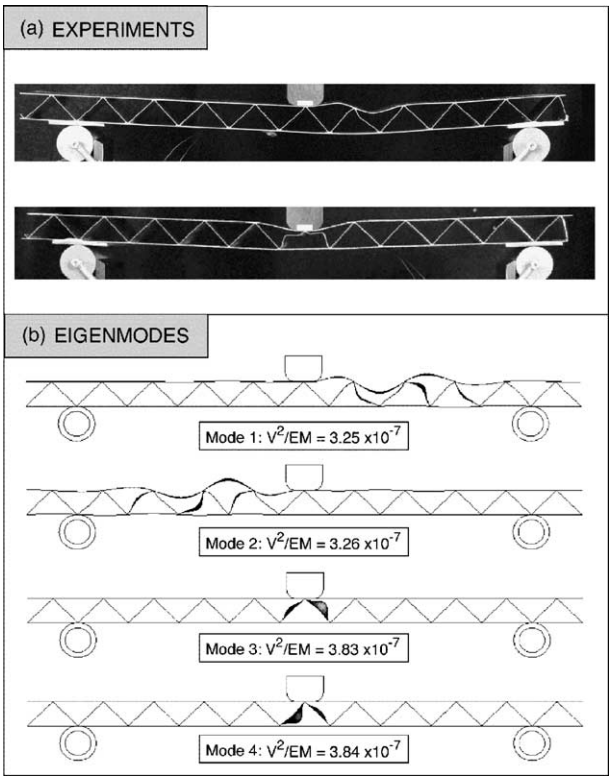


Fig. 11. (a) Experimental results for two nominally identical tests performed on the thicker panel in the transverse direction, revealing markedly different deformation modes. (b) Eigenmodes and associated critical loads from FE calculations. Note that mode 1 buckling is consistent with the first of the two test specimens whereas mode 3 is representative of the second.

(Valdevit et al., 2004) and the provision of information about the behavior subsequent to failure initiation. Two sets of panels were tested in both longitudinal and transverse orientations. The designs were chosen based on failure maps, developed using the analytical model. Each of the two panel types was near-optimal in one of the two directions. The main findings can be summarized as follows:

(a) Comparisons with measurements and finite element simulations have affirmed that the analytic model provides an accurate assessment of the critical loads when controlled by face yielding. Buckling loads are more difficult to predict accurately, because of their sensitivity to the rotational constraints of the nodes as well as fabrication imperfections.
(b) The assessment of panels tested under longitudinal loading has revealed the importance of compressive stresses beneath the platen. To incorporate this effect, a core indentation model based on beam theory has been derived and shown to be in good agreement with experimental results.
(c) The behavior subsequent to failure initiation depends strongly on the position of the panel in the failure map. Designs that lie deep within face yielding are the only ones to exhibit appreciable hardening. All other designs buckle (either elastically or plastically), causing softening soon after the criticality. Thus, when robustness is a key requirement, off-optimum designs are preferred.
(d) Panels subjected to transverse loads are imperfection sensitive. For designs near the confluence of core and face buckling, such imperfections can trigger modes that differ from analytic expectations. Panels subjected to longitudinal loads exhibit only weak imperfection sensitivity.

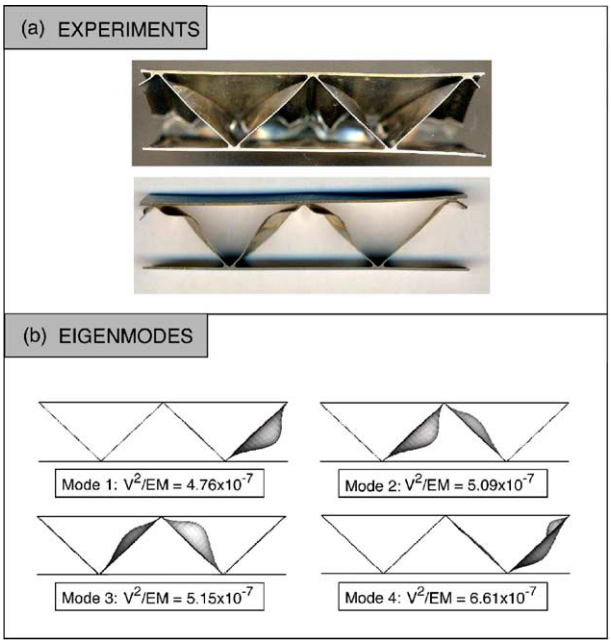


Fig. 12. (a) Experimental results for two nominally identical tests performed on the thicker panel in the longitudinal direction, showing quite similar deformation modes. (b) Eigenvalue analysis with the gour lowest modes depicted.

(e) The finite element calculations predict the limit loads quite successfully, although they under-predict the extent of plastic deformation.

## Acknowledgements

This work was supported by ONR, through both the MURI program on Blast Resistant Structures through a sub-contract from Harvard University to the UCSB (Contract No. 123163-03), and the program on Multifunctional Implementations of Topologically Structured Materials through a sub-contract from the University of Virginia to UCSB (Contract No. GG10376-114969).

## Appendix A. Core indentation model

To ascertain the indentation stresses, the core is modeled as a homogeneous elastic material with an *effective* through-thickness stiffness $k$. For corrugated cores, elementary geometry gives:

$$k = \frac{d_c E \sin^4\theta}{H_c^2 \cos\theta} \tag{A.1}$$

The load is transmitted to the core through deformation of the face sheet. From beam theory, the normalized face deflection, $\hat{\delta} \equiv \delta k a/p$, at normalized position, $\hat{x} \equiv x/a$, subject to an applied pressure $p$ over a length $2a$ (the platen width) is described by the differential equations:

$$\begin{aligned} &\frac{d^4\hat{\delta}}{d\hat{x}^4} + \beta^4\delta = -\beta^4 \quad \text{for } 0 \leqslant \hat{x} \leqslant 1 \\ &\frac{d^4\hat{\delta}}{d\hat{x}^4} + \beta^4\delta = 0 \qquad \text{for } \hat{x} > 1 \end{aligned} \tag{A.2}$$

where

$$\beta \equiv a\left[\frac{12\sin^4\theta}{\cos\theta}\frac{d_c}{H_c^2 d_f^3}\right]^{1/4} \tag{A.3}$$

Solution of these equations yields the *effective* stress within the core (treating it as a homogeneous continuum):

$$\begin{aligned} \frac{\sigma_{eff}}{p} = -1 - \frac{1}{2}\Bigg\{ & e^{-\frac{\sqrt{2}}{2}\beta(\hat{x}+1)}\left[\sin\left(\frac{\sqrt{2}}{2}\beta\right)\sin\left(\frac{\sqrt{2}}{2}\beta\hat{x}\right) - \cos\left(\frac{\sqrt{2}}{2}\beta\right)\cos\left(\frac{\sqrt{2}}{2}\beta\hat{x}\right)\right] + e^{\frac{\sqrt{2}}{2}\beta(\hat{x}-1)} \\ & \times\left[\sin\left(\frac{\sqrt{2}}{2}\beta\right)\sin\left(\frac{\sqrt{2}}{2}\beta\hat{x}\right) + \cos\left(\frac{\sqrt{2}}{2}\beta\right)\cos\left(\frac{\sqrt{2}}{2}\beta\hat{x}\right)\right]\Bigg\} \end{aligned} \tag{A.4(a)}$$

for $\hat{x} \leqslant 1$ and

$$\frac{\sigma_{eff}}{p} = -\frac{1}{2}e^{-\frac{\sqrt{2}}{2}\beta(\hat{x}+1)}\left[\left(1+e^{\sqrt{2}\beta}\right)\sin\left(\frac{\sqrt{2}}{2}\beta\right)\sin\left(\frac{\sqrt{2}}{2}\beta\hat{x}\right) + \left(e^{\sqrt{2}\beta}-1\right)\cos\left(\frac{\sqrt{2}}{2}\beta\right)\cos\left(\frac{\sqrt{2}}{2}\beta\hat{x}\right)\right] \tag{A.4(b)}$$

for $\hat{x} > 1$. Representative stress distributions are plotted on Fig. A.1(a). The maximum values are obtained near the origin. Upon setting $\hat{x} = 0$ in Eq. (A4), an analytic estimate of the peak stress is obtained:

$$\frac{\sigma_{max}}{p} = f(\beta) = -1 + e^{-\frac{\beta}{\sqrt{2}}}\cos\left(\frac{\beta}{\sqrt{2}}\right) \tag{A.5}$$

This result is plotted in Fig. A.1(b). Note that the stress becomes more localized as $\beta$ increases. Specifically, when $\beta \ll 1$, the faces are sufficiently stiff to distribute the pressure over a large portion of the core, effectively eliminating the stress concentrating effect of the loading platen. Otherwise, for $\beta \gg 1$, the faces are ineffective at load spreading and the pressure is transmitted in its entirety to the core directly beneath the platen.

The normal stress $\sigma_c$ in a member of a corrugated core can be related to the effective stress $\sigma_{eff}$ via:

$$\sigma_c = \frac{(H_c + d_f)\cos\theta}{d_c\sin^2\theta}\sigma_{eff} \tag{A.6}$$

Its maximum value (from Eqs. (A.5) and (A.6)) is

$$\sigma_{c,max} = \frac{(H_c + d_f)\cos\theta}{d_c\sin^2\theta}\frac{Vf(\beta)}{a} \tag{A.7}$$

Fig. A.2 shows a comparison between the indentation stress distribution predicted by this model and the results of a three-dimensional finite element calculation for the thicker panel used in the present study. A mesh similar to that depicted in Fig. 6 was used for the FEA. The compressive stress in the core web close to the indented face sheet was extracted and Eq. (A.6) was then used to ascertain the effective stress. In this case, the maximum value is predicted reasonably well by the analytical model (within about 20%), although

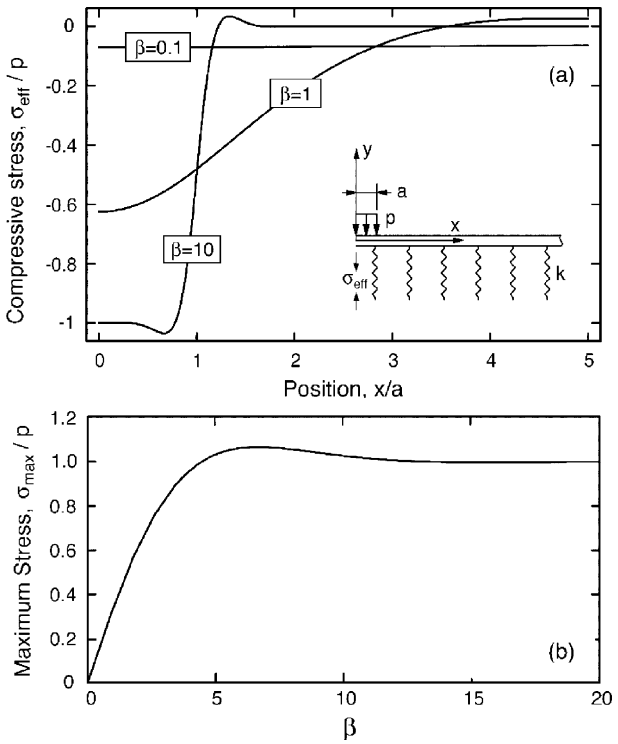


Fig. A.1. Effects of the non-dimensional parameter $\beta$ on the stress intensification under the loading platen. For $\beta > 5$, the indentation stress is transmitted directly to the core beneath the platen.

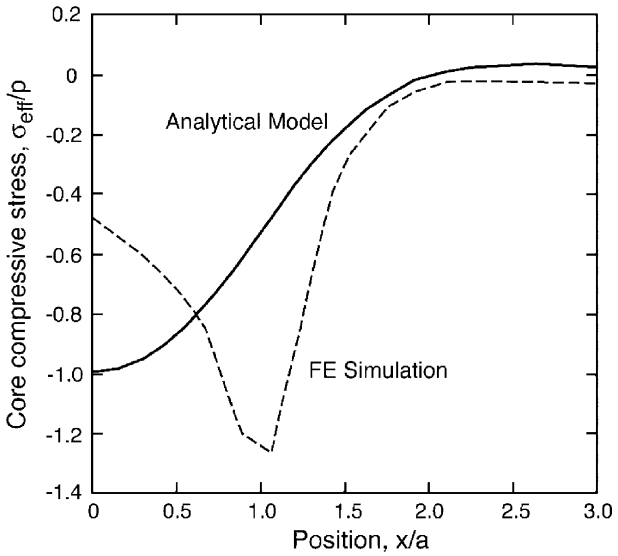


Fig. A.2. Comparison of numerical and analytical results for the compressive stress in the core due to the loading platen in a panel loaded in the longitudinal direction.

the location of the peak is shifted somewhat. The latter shift is not unexpected, since the analytical model assumes a uniform pressure on the top face and thus does not capture the details of the indenter–panel contact.

Combining the stresses from generalized bending and indentation with the von Mises yield criterion gives:

$$\sigma_{\mathrm{b,max}}^2 + \sigma_{\mathrm{c,max}}^2 - \sigma_{\mathrm{b,max}}\sigma_{\mathrm{c,max}} + 3\tau_{\mathrm{max}}^2 = \sigma_{\mathrm{Y}}^2 \tag{A.8}$$

where $\sigma_{\mathrm{b,max}}$ and $\tau_{\mathrm{max}}$ are the maximum values due to the bending moment and the applied shear (Valdevit et al., 2004). The resulting yield load for the corrugated core in the longitudinal orientation is

$$\left(\frac{V^2}{EM}\right)_{\mathrm{CY}} = \min_{y\in\left[0,\frac{H_c}{2}\right]}\left\{\frac{\sigma_{\mathrm{Y}}/E}{\sqrt{\alpha_{\mathrm{b}}+\alpha_{\mathrm{i}}+\alpha_{\mathrm{c}}+\alpha_{\mathrm{s}}}}\right\} \tag{A.9}$$

where the $\alpha$ coefficients are given by:

$$\begin{aligned}
\alpha_{\mathrm{b}} &= \frac{4(y/(H_{\mathrm{c}}+d_{\mathrm{f}}))^2}{\left(\frac{H_{\mathrm{c}}}{l}+\frac{d_{\mathrm{f}}}{l}\right)^2\left(\frac{d_{\mathrm{f}}}{l}+\frac{1}{6\cos\theta}\frac{d_{\mathrm{c}}}{l}\right)^2}\\
\alpha_{\mathrm{i}} &= \frac{\cos^2\theta}{\sin^4\theta}f^2(\beta)\left(\frac{H_{\mathrm{c}}}{l}+\frac{d_{\mathrm{f}}}{l}\right)^2\Bigg/\left[\left(\frac{d_{\mathrm{c}}}{l}\right)^2\left(\frac{a}{l}\right)^2\right]\\
\alpha_{\mathrm{c}} &= -\frac{2\cos\theta}{\sin^2\theta}f(\beta)\frac{y}{H_{\mathrm{c}}+d}\Bigg/\left[\left(\frac{d_{\mathrm{f}}}{l}+\frac{1}{6\cos\theta}\frac{d_{\mathrm{c}}}{l}\right)\frac{d_{\mathrm{c}}}{l}\frac{a}{l}\right]\\
\alpha_{\mathrm{s}} &= 3\left[\frac{1}{\tan\theta}\frac{d_{\mathrm{f}}}{l}\Bigg/\frac{d_{\mathrm{c}}}{l}+\frac{1}{\sin\theta}\left(\frac{1}{4}-\left(\frac{y}{H_{\mathrm{c}}+d_{\mathrm{f}}}\right)^2\right)\right]^2\Bigg/\left(\frac{d_{\mathrm{f}}}{l}+\frac{1}{6\cos\theta}\frac{d_{\mathrm{c}}}{l}\right)^2
\end{aligned} \tag{A.10}$$

Ideally, to predict core buckling, an approach that combines all stress components (due to bending moment, shear and indentation) would be used in combination with an appropriate plate buckling criterion: analogous to the preceding approach used for core yielding. Although such solutions are available (Shahabian and Roberts, 1999), the results are too cumbersome to be used in the present design studies. Instead, a simpler (although less accurate) approach is adopted. Specifically, the critical load for core buckling under the indentation stress (absent shear and bending moment) is computed. This load is then compared with that due to combined bending moment and shear (Eq. (5d)). The lower of the two values is used as the buckling load. In non-dimensional form, the buckling load for indentation alone is

$$\left(\frac{V^2}{EM}\right)_{\mathrm{CB}} = \frac{\pi^2\sin^2\theta}{3(1-\nu^2)\cos\theta}\frac{1}{f(\beta)}\left(\frac{d_{\mathrm{c}}}{l}\right)^3\frac{l}{(H_{\mathrm{c}}+d_{\mathrm{f}})}\left(\frac{l}{\min(\frac{H_{\mathrm{c}}}{\sin\theta},2a)}\right)^2\frac{a}{l} \tag{A.11}$$

The results in Eqs. (A.9), (A.10), (A.11) were combined with those in Eq. (5) to construct the modified mechanism map in Fig. 3 and to provide analytic estimates of the critical loads for the tested designs.

## References

Ashby, M.F., Evans, A.G., Fleck, N.A., Gibson, L.J., Hutchinson, J.W., Wadley, H.N.G., 2000. Metal Foams: A Design Guide. Butterworth-Heinemann.

Bazant, Z.P., Cedolin, L., 1991. Stability of Structures. Oxford University Press.

Chiras, S., Mumm, D.R., Evans, A.G., Wicks, N., Hutchinson, J.W., Dharmasena, K., Wadley, H.N.G., Fichter, S., 2002. The structural performance of near-optimized truss core panels. International Journal of Solids and Structures 39 (15), 4093–4115.

Cote, F., Deshpande, V., Fleck, N.A., Evans, A.G., 2004. The out-of-plane compressive behavior of metallic honeycombs. Materials Science and Engineering A—Structural Materials Properties Microstructure and Processing 380 (1–2), 272–280.

Evans, A.G., Hutchinson, J.W., Fleck, N.A., Ashby, M.F., Wadley, H.N.G., 2001. The topological design of multifunctional cellular metals. Progress in Materials Science 46, 309–327.

Fleck, N.A., Deshpande, V.S., 2004. The resistance of clamped sandwich beams to shock loading. Journal of Applied Mechanics—Transactions of the ASME 71 (3), 386–401.

Lu, T.J., Valdevit, L., Evans, A.G., 2005. Active cooling by metallic sandwich structures with periodic cores. Progress in Materials Science 50 (7), 789–815.

Qiu, X., Deshpande, V.S., Fleck, N.A., 2003. Finite element analysis of the dynamic response of clamped sandwich beams subject to shock loading. European Journal of Mechanics A—Solids 22 (6), 801–814.

Qiu, X., Deshpande, V.S., Fleck, N.A., 2004. Dynamic response of a clamped circular sandwich plates to shock loading. Journal of Applied Mechanics, ASME 71 (5), 637–645.

Radford, D.D., Deshpande, V.S., Fleck, N.A., in press. The response of clamped sandwich beams subjected to shock loading. International Journal of Impact Engineering.

Rathbun, H.J., Wei, Z., He, M.Y., Zok, F.W., Evans, A.G., Sypeck, D.J., Wadley, H.N.G., 2004. Measurement and simulation of the performance of a lightweight metallic sandwich structure with a tetrahedral truss core. Journal of Applied Mechanics 71 (5), 368–374.

Rathbun, H.J., Zok, F.W., Evans, A.G., in press. Strength optimization of metallic sandwich panels subject to bending. International Journal of Solids and Structures, doi:10.1016/j.ijsolstr.2005.06.044.

Shahabian, F., Roberts, T.M., 1999. Buckling of slender web plates subjected to combinations of in-plane loading. Journal of Constructional Steel Research 51, 99–121.

Sypeck, D.J., Wadley, H.N.G, 2001. Multifunctional micro-truss laminates: Textile synthesis and properties. Journal of Materials Research 16 (3), 890–897.

Valdevit, L., Hutchinson, J.W., Evans, A.G., 2004. Structurally optimized sandwich panels with prismatic cores. International Journal of Solids and Structures 41 (18–19), 5105–5124.

Vaughn, D., Canning, M., Hutchinson, J.W., 2005. Coupled plastic wave propagation and column buckling. Journal of Applied Mechanics, ASME 72 (1), 139–146.

Wadley, H.N.G., Fleck, N.A., Evans, A.G., 2003. Fabrication and structural performance of periodic cellular metal sandwich structures. Composites Science and Technology 63 (16), 2331–2343.

Wicks, N., Hutchinson, J.W., 2001. Optimal truss plates. International Journal of Solids and Structures 38, 5165–5183.

Wicks, N., Hutchinson, J.W., 2004. Performance of sandwich plates with truss cores. Mechanics of Materials 36 (8), 739–751.

Xue, Z.Y., Hutchinson, J.W., 2003. Preliminary assessment of sandwich plates subject to blast loads. International Journal of Mechanical Sciences 45 (4), 687–705.

Xue, Z.Y., Hutchinson, J.W., 2004. A comparative study of impulse-resistant metal sandwich plates. International Journal of Impact Engineering 30 (10), 1283–1305.

Zok, F.W., Rathbun, H.J., Wei, Z., Evans, A.G., 2003. Design of metallic textile core sandwich panels. International Journal of Solids and Structures 40 (21), 5707–5722.

Zok, F.W., Waltner, S.A., Wei, Z., Rathbun, H.J., McMeeking, R.M., Evans, A.G., 2004. A protocol for characterizing the structural performance of metallic sandwich panels: application to pyramidal truss cores. International Journal of Solids and Structures 41 (22–23), 6249–6271.

Zok, F.W., Rathbun, H.J., He, M., Ferri, E., Mercer, C., McMeeking, R.M., Evans, A.G., in press. Structural performance of metallic sandwich panels with square honeycomb cores. Philosophical Magazine.